

COMPARATIVE STUDY OF FLOW TESTS AND CFD SIMULATIONS IN A HYDRAULIC ENERGY DISSIPATOR WITH GEAR GEOMETRY

BRIONES REYES ALEXIS RENATO

CIVIL ENGINEERING UNDERGRADUATE STUDENT, UNIVERSIDAD PRIVADA DEL NORTE, FACULTY OF ENGINEERING, LIMA, PERÚ.

EMAIL: n00361489@upn.pe, ORCID ID: HTTPS://ORCID.ORG/0000-0001-8805-6487

CARMONA ARTEAGA ABEL

MASTER OF SCIENCE IN WATER RESOURCES, UNIVERSIDAD PRIVADA DEL NORTE, FACULTY OF ENGINEERING, LIMA, PERÚ.

EMAIL: abel.carmona@upn.edu.pe, ORCID ID: HTTPS://ORCID.ORG/0000-0003-2895-9582

Abstract—This research combines experimental tests and CFD simulations in Autodesk to model a gear-shaped energy dissipator. The objective is to evaluate the accuracy of the CFD simulation in replicating laminar and turbulent flow patterns observed in the laboratory, using water as the test fluid. The methodology includes designing in AutoCAD and testing on a flow table, recording data on flow and pressure. Results showed kinematic consistency between simulation and experiment, reflecting similar flow patterns and pressure behavior. Minor discrepancies are attributed to unmodeled factors such as bubbles and vibrations. The conclusions highlight that reducing drag increases energy efficiency and that controlling lift is crucial for design stability. This integration of tests and simulations not only validates CFD as a predictive tool but also supports its application in the design of hydraulic structures to mitigate floods, particularly relevant in the context of mitigating landslides (huaycos) in Peru.

Keywords: Energy dissipator, CFD simulations, flow tests, geometric similarity, kinematic similarity.

INTRODUCTION

Climate change, driven by the increase in greenhouse gases, has intensified phenomena such as extreme rainfall and prolonged droughts, disrupting global precipitation patterns [1]. The rise in the frequency and magnitude of extreme rainfall is one of the most evident consequences of climate change, particularly in tropical and Mediterranean regions [2]. These intense rains increase the flow and speed of rivers, creating a higher risk of bank erosion and flooding, which affects both the environment and the safety of human populations. In Peru, for example, intense rainfall has caused recurrent flooding and river overflows, where nearby communities are exposed to a high risk of natural disasters [3]. The magnitude of these events highlights the urgent need to address the challenges posed by climate change and its effects on infrastructure and human life.

In the Peruvian context, huaycos — sudden floods involving intense flows — represent a constant threat to both the population and infrastructure, especially in areas where urbanization has grown haphazardly near riverbeds and mountain slopes [6]. These huaycos are triggered by heavy rainfall and manifest as the rapid drainage of torrential water, which leads to accelerated erosion. The currents carry large blocks of rock, devastating homes and infrastructures such as basic service networks, causing interruptions in water, electricity, and communication supplies, in addition to significant human and economic losses [4]. The impact of these events is worsened by the social and economic problems they cause, including street flooding, overflow of channels, environmental pollution, and erosion of agricultural land [5]. Figure 1 illustrates the magnitude of the flow that a huayco can generate.



Fig. 1 Huaycos in Peru [7]

To address this issue, it is essential to delve into the study of structures capable of dissipating the energy generated



by fluids, thus reducing the damage they may cause.

This reality raises an important question:

Why, to date, are there so few projects dedicated to the development of structures for dissipating the energy generated by fluids?

A reasonable answer to this question is the limited knowledge available on the subject, the scarce information, and the intrinsic complexity of fluid dynamics. This field of study requires a detailed analysis of fluid kinematics, which is known for its difficulty due to the need to solve complex differential equations. Among these, the Navier-Stokes equation stands out, as it describes the behavior of fluids and presents significant challenges for its practical application in the design of energy dissipation structures.

Currently, advanced software has been developed that allows for a deeper understanding of fluid dynamics. One example is Autodesk CFD, which has made a positive impact in this field by facilitating the search for potential solutions through modeling and the incorporation of various parameters.

I. RESEARCH OBJECTIVE

Therefore, this research presents itself as a comparative study that integrates experimental tests, conducted on a flow table in a laboratory, and computational simulations using Autodesk CFD software. The objective of this study is to model and analyze in CFD a concrete structure in the shape of a gear, designed as a hydraulic energy dissipation device, in order to observe and compare the behavior of laminar and turbulent flow under controlled conditions. The models will be subjected to tests using water as the working fluid, allowing for a detailed assessment of the accuracy and effectiveness of the CFD results compared to the experimental tests.

II. THEORETICAL FRAMEWORK

A.Autodesk Inventor

Autodesk's 3D CAD program for mechanical modeling, simulation, and visualization of complex projects. It allows for the integration of 2D and 3D data, product validation before manufacturing, and includes tools for parametric design and simulation [8].

B. Autodesk CFD

A software for computational fluid dynamics simulation. It enables the analysis of fluid flow, heat transfer, and movement, optimizing designs and reducing the need for physical prototypes. It integrates with other Autodesk products to enhance efficiency in sectors such as cooling and HVAC systems [9].

C. Meshing in CFD

In CFD, meshing is the discretization of the model, composed of nodes and edges that form a surface or volume mesh, made up of elements like triangles, tetrahedra, or pyramids. Fluid properties are calculated at the nodes and interpolated along the edges. Meshes can be structured, for simple geometries, or unstructured, for complex shapes. A finer mesh increases accuracy but also computational load [10].

D.Drag Force

Drag is a force generated by the flow of a fluid that opposes the motion of an object. To maintain or increase speed, it is necessary to counteract this force by propulsion in the opposite direction, which requires additional energy consumption. Therefore, minimizing drag is a key strategy to optimize energy efficiency [11].

$$F_{D} = C_{D} \times \frac{\rho \times V^{2}}{2} \times A \tag{1}$$

Where F_D is the drag force, C_D is the drag coefficient, ρ is the fluid density, A is the characteristic area of the body, and V is the free-stream velocity of the fluid.

E. Lift Force

Lift is a force generated by a fluid, acting in a direction perpendicular to the motion of an object [11].

In this study, lift is defined as the force exerted by the fluid flow perpendicular to the path of the energy dissipation device. Considering lift is essential in the design of these devices to ensure their stability and effectiveness.

F. Stagnation Point

A stagnation point is the location in a fluid flow where the fluid velocity is reduced to zero, and pressure reaches its maximum, known as stagnation pressure. At this point, a force is generated opposite to the motion of the body, resulting in drag force. The magnitude of this force depends not only on the stagnation pressure but also on the pressure at the rear of the body, making it difficult to predict the total drag without using the drag coefficient [11]. G.Separation Point

The separation point is where the fluid flow detaches from the surface of the body, causing a change in flow direction and the formation of a wake. By moving the separation point toward the rear of the body, the size of the wake can be reduced, which in turn decreases pressure drag. This concept is crucial in the process of aerodynamics, where the goal is to optimize the shape of the body to improve aerodynamic performance and reduce drag, often referred to as form drag [11].

H.Wake

A wake is the turbulent disturbance in a fluid caused by the passage of a body, generating two types of drag: pressure drag, due to the low pressure behind the body, and friction drag, caused by shear stresses in the boundary layer adhered to the surface. The characteristics of the wake depend on the shape of the body, the Reynolds number, and the surface roughness. Improving aerodynamic design, such as rounding corners, can reduce the wake and total drag, enhancing flow efficiency [11]. This disturbance is illustrated in Figure 2.



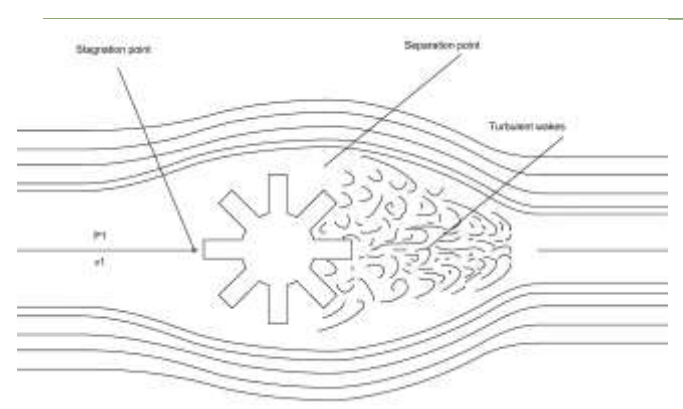


Fig. 2 Stagnation point, separation point, and turbulent wakes

I. Reynolds number

The Reynolds number (N_R) is a dimensionless number used to predict the behavior of fluid flow, particularly in terms of whether the flow is laminar or turbulent [11].

$$N_{R} = \frac{\rho \, v \, D}{u} \tag{2}$$

 N_R is the Reynolds number, v is the flow velocity, D is the hydraulic diameter, and μ is the dynamic viscosity.

$$D = \frac{4ab}{2a+b} \tag{3}$$

Where: a is the height of the wetted area, and b is the length of the wetted area.

J. Laminar and turbulent flow

Laminar and turbulent flows exhibit distinctive behaviors in fluid dynamics, largely defined by the Reynolds number. In laminar flow, particles move in an orderly manner in parallel layers with constant velocity, characteristic of low speeds and low Reynolds numbers; in civil structures like bridges, this type of flow can induce lateral forces and vibrations due to particle alignment as they interact with obstacles [12]. On the other hand, turbulent flow is chaotic and disordered, with high mixing of particles and vortex formation, prevailing in conditions with a high Reynolds number. Although turbulent flow doesn't produce as noticeable transverse forces, it can increase drag on bridge piers by generating higher pressure and thrust against obstacles [12]. Its complex modeling uses advanced tools such as Large Eddy Simulation (LES) and Finite Element Method (FEM) [13].

K.Law of Similarity

Geometric similarity between a physical model and its prototype occurs when both have identical shapes and only differ in size by a constant scale factor of lengths, known as λ . This factor ensures that the ratio between homologous lengths is constant, guaranteeing proportional distances and equal angles [14]. However, in practice, it may be necessary to distort the scale in one direction, usually vertical, to make the model more manageable [15].

Kinematic similarity occurs when a model and its prototype maintain a constant relationship between dynamic pressures at corresponding points, and the streamlines are geometrically similar [14]. This means that velocities and accelerations at homologous points are proportional and maintain a direction parallel to the flow. Kinematic similarity depends on time scale and homologous lengths, implying specific relations between time, velocity, acceleration, and flow rate [15]. It is important to note that geometric similarity is necessary but not sufficient for kinematic similarity; additional criteria must be met [16].

Dynamic similarity is achieved when, in addition to geometric and kinematic similarity, there is a constant relationship between inertia forces at corresponding points. This ensures that the acting forces in both flows are parallel and proportional in magnitude, allowing the ratio between homologous forces to be equal at each point [14]. To guarantee dynamic similarity, the mass and density distributions must be equivalent, ensuring that the force polygons are geometrically similar [16].

L. Navier-Stokes Equation

The Navier-Stokes equation describes the movement of fluids, integrating pressure and viscosity forces. It is derived from Cauchy's equation, which contains a stress tensor with 9 components. To simplify it, constitutive equations are introduced, which relate viscous stresses to velocity and fluid properties. In the case of an incompressible and Newtonian fluid, constant density and viscosity assumptions simplify the equation to a nonlinear and unsteady form that describes how fluid velocity is affected by pressure and viscosity. To attempt solving it, the continuity equation must be used [17].

$$\rho \frac{D\vec{v}}{D_t} = -\vec{\nabla}_P + \rho \vec{g} + \mu \nabla^2 \vec{v}$$
 (4)

Where: ρ is the fluid density, $D\vec{v}/D_t$ is the total rate of change of velocity, $-\nabla P$ is the pressure gradient driving the flow $y \rho g^{2}$ is the gravitational force per unit volume. The viscosity μ measures the internal resistance to motion, while $\nabla^2 \vec{v}$ represents the diffusion of velocity due to viscosity.

M. Vorticity

Vorticity measures the local rotation of a fluid at a point in the flow. In incompressible and inviscid fluids, it is generated at solid surfaces by the no-slip condition, creating boundary layers and wakes. At high Reynolds numbers, vorticity concentrates in rotational flow zones, such as boundary layers and wakes, while the rest of the flow is

Open Access

irrotational [18].

N.General Energy Equation

The general energy equation is an extension of Bernoulli's equation, used to address problems where energy losses and gains occur in a flow system [11].

$$\frac{v_1^2}{2g} + \frac{P_1}{\gamma} + z_1 = \frac{v_2^2}{2g} + \frac{P_2}{\gamma} + z_2 + h_t \tag{5}$$

The inlet velocity (v_1) and outlet velocity (v_2) , along with the inlet pressure (P_1) and outlet pressure (P_2) , refer to the fluid conditions at two sections of a conduit. The elevations at these sections are denoted as z_1 and z_2 . Gravity (g) and specific weight (γ) are expressed in m/s² and N/m³, respectively. The total losses (hT) represent the energy lost due to friction and other factors in the system.

O.Continuity Equation for Fluids

The continuity equation ensures that, in a steady flow, the volumetric flow rate is constant at any section, applicable also to gases at velocities less than 100 m/s with minimal error [11].

$$A_1 v_1 = A_2 v_2 \tag{6}$$

A1 and A2 are the cross-sectional areas at two different points in the conduit, while v1 and v2 are the fluid velocities at those sections.

P. Laminar Flow Table

A laminar flow table is an experimental device that allows for the observation and adjustment of bidimensional fluid flow, useful for studying heat transfer and validating fluid dynamics principles [19].

METHOD

The research methodology is developed through an experimental and theoretical approach, beginning with the design of a concrete structure in AutoCAD, followed by modeling in computational fluid dynamics (CFD) software. Subsequently, a physical model will be fabricated and tested on a laminar flow table using water as the test fluid. During this phase, flow patterns and relevant variables will be recorded. Finally, the results obtained from the CFD simulations will be analyzed and compared with the experimental data collected, enabling the validation of the simulations' accuracy and contributing to the understanding of the flow behavior around the concrete structure.

Q. Modeling in AutoCAD

In this stage, a figure will be designed consisting of a central circle with a radius of 2 cm (4 cm diameter), from which eight rectangles extend in equidistant directions. Each rectangle measures 1 cm in width and 8 cm in length, positioned so that its center aligns with the center of the circle. This arrangement causes the rectangles to intersect the central circle and extend outward, forming a symmetrical shape resembling a gear. The described design is illustrated in Figure 3.

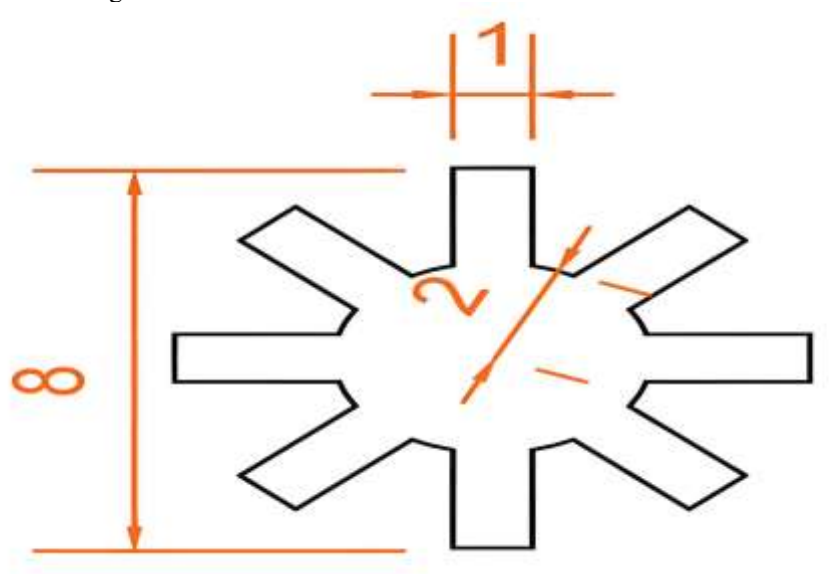


Fig. 3 Design of the block in AutoCAD

With the design established, we proceed to generate the block's layout. To do this, we begin by drawing the flow table, which has dimensions of 49.5 cm in width and 75 cm in length. These values will be used to trace the rectangle representing the table. Next, we will position the block so that its center is 5 cm from the edge in the width direction and 4 cm from the edge in the length direction. With this arrangement, we will use the Array command, specifying the distances between blocks and the number of rows and columns, setting a total of 65 columns and -41.5 rows. Figure 4 illustrates the described layout.



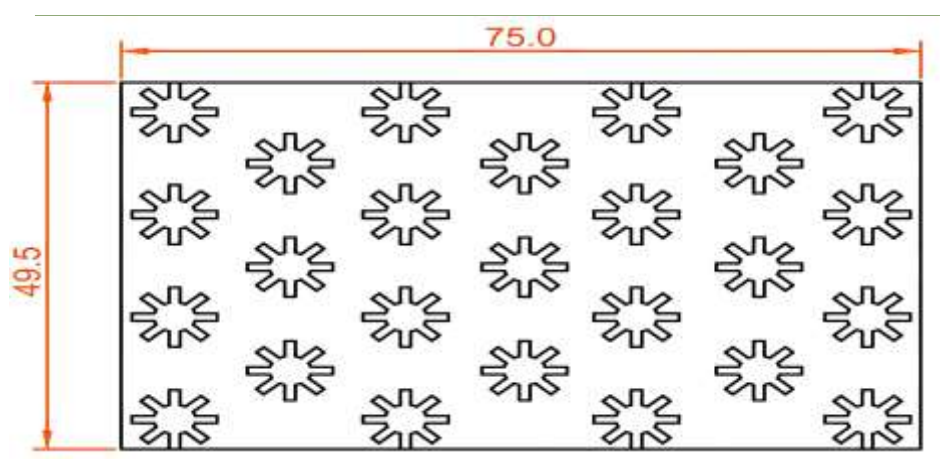


Fig. 4 Block distribution in AutoCAD

R. Modeling in Autodesk Inventor

In this stage, we will draw the rectangle representing the flow table in Inventor, using the previously mentioned dimensions. We will divide this rectangle with a diagonal line and then apply the construction command. Next, we will use the coincidence constraint to align the necessary elements. With this preparation, we will be able to easily copy our design from AutoCAD to Inventor and adjust it within the rectangle. Finally, we will generate the Patch to proceed with the CFD simulation in the next stage.

S. Concrete Model Fabrication

In this stage, 25 high-density Styrofoam molds will be created with a thickness of 5 cm and the specified measurements. A mixture of concrete, gypsum, and water will be prepared in a 1:2:1 ratio and poured into the molds. Once dry, the mixture will be de-molded, and the blocks will be polished if necessary, maintaining maximum geometric precision for accurate analysis. Figure 5 illustrates the drying process in the molds and the de-molded dissipators.



Fig. 5 Molding and de-molding process

T. Laminar Flow Table Test

The concrete dissipators will be placed on a laminar flow table over an acrylic sheet, following the design for CFD comparison; water with powder and fluorescent lighting will visualize turbulence, contained by wooden edges (49.5 \times 75 cm); heights will be measured with a ruler, times with stopwatches, and inlet height recorded to calculate area and viscosity, as shown in Fig. 6.



Fig. 6 Block distribution on the laminar flow table

In Figure 7, the procedure followed in the laboratory for laminar and turbulent flows is described, with the objective



of obtaining the Reynolds number and verifying the type of flow.

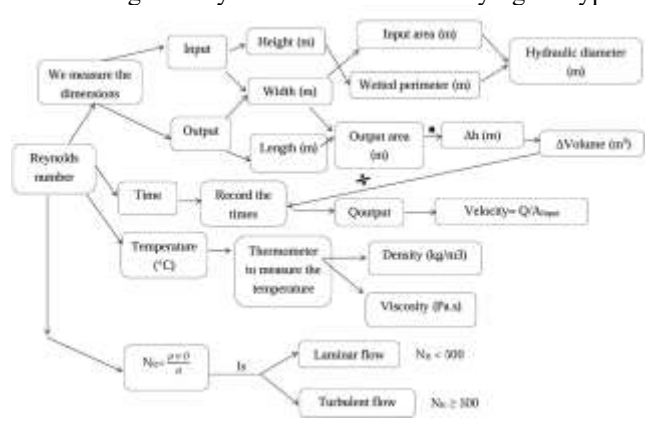


Fig. 7 Flowchart of laboratory steps for simulations

RESULTS

U.Laminar Flow

Four people (T-A, T-B, T-C, and T-D) recorded partial times corresponding to height increments (Δh) of 0.01 m. This is reflected in Table I.

TABLE I PARTIAL TIME RECORDINGS FOR LAMINAR FLOW

H accumulated (m)	T-A (s)	T-B (s)	T-C (s)	T-D (s)	Average partial time (s)
0.01	21.41	21.36	21.26	21.27	21.325
0.02	22.19	21.79	21.53	22.17	21.920
0.03	23.87	24.13	24.46	23.96	24.105
0.04	22.25	22.47	22.3	22.19	22.303
0.05	24.42	24.48	24.43	24.51	24.460
0.06	23.55	23.6	23.78	23.87	23.700
0.07	22.76	22.38	22.25	22.65	22.510
0.08	22.46	22.61	22.6	22.38	22.513
0.09	20.19	20.44	20.22	20.13	20.245
0.1	20.57	20.11	20.38	20.26	20.330

Then, the average of these times was calculated for each Δh and will be presented as Δ time values in Table II. In Table II, the volume variation (Δ Volume) was calculated as the product of the base area (0.0558 m²) and a height variation of 0.01 m, yielding 0.000558 m³. The outflow rate (Q out) was estimated by dividing Δ Volume by the recorded partial time (for example, 21.325 s), resulting in 2.61665 × 10⁻⁵ m³/s. Using the flow conservation principle (Q in = Q out), the inlet velocity (V in) was calculated by dividing Q out by the inlet area (0.002475 m²), obtaining 0.01057 m/s. These calculations help evaluate the flow behavior based on partial times and height variations.

TABLE II CALCULATION OF THE INLET VELOCITY FOR LAMINAR FLOW

H	Λh	Δ	Δ	Q	Inflow
accumula	(m)	time	Volum	outflow	velocity
ted (m)	(111)	(s)	e (m3)	(m3/s)	(m/s)
0.01	0.0	21.32	0.0005	0.000026	0.011
0.01	1	5	58	0.000020	0.011
0.02	0.0	21.92	0.0005	0.000025	0.010
0.02	1	0	58	0.000023	0.010
0.03	0.0	24.10	0.0005	0.000023	0.009
0.03	1	5	58	0.000023	0.009
0.04	0.0	22.30	0.0005	0.000025	0.010
0.04	1	3	58	0.000023	0.010
0.05	0.0	24.46	0.0005	0.000023	0.009
0.03	1	0	58	0.000023	0.009



0.06	0.0	23.70	0.0005 58	0.000024	0.010
	0.0	22.51			
0.07	1	0	0.0005 58	0.000025	0.010
0.08	0.0	22.51	0.0005 58	0.000025	0.010
	1	3			
0.09	0.0	20.24	0.0005 58	0.000028	0.011
0.1	0.0	20.33	0.0005 58	0.000027	0.011

TABLE III AVERAGES OF OUTFLOW RATE AND INLET VELOCITY FOR LAMINAR FLOW

Q average outflow	m ³ /s	2.50733E-05
V average inflow	m/s	0.0101

In this study, the density of water was determined from the recorded temperature of 19°C using the formula $\rho_{\text{Water}} = 1000 - \frac{(19-4)^2}{180}$, yielding a value of 998.75 kg/m³. The average inlet velocity, taken from Table III, is 0.0101 m/s. Additionally, the hydraulic diameter was calculated using equation (3), resulting in a value of 0.0196 m.

The dynamic viscosity (Pa·s) was determined by interpolation using the values from Table A.1 of the Fluid Mechanics book by Robert L. Mott. For a temperature of 18.75°C, the viscosities corresponding to 15°C and 20°C were interpolated, yielding a value of 0.001046 Pa·s.

To determine the Reynolds number, the following values were used: a density of 998.75 kg/m³, a flow velocity of 0.0101 m/s, a hydraulic diameter (Dh) of 0.0196 m, and a dynamic viscosity (η) of 0.001 Pa·s. These parameters allow for the calculation of the flow regime in the analyzed system.

Finally, the Reynolds number was calculated using equation (2), resulting in a value of 189.629, which confirms that the flow is laminar.

V. Turbulent Flow

Four people (T-A, T-B, T-C, and T-D) recorded partial times for height increments (Δh) of 0.01 m. This is reflected in Table IV.

TABLE IV PARTIAL TIME RECORDINGS FOR TURBULENT FLOW

H accumulated (m)	T-A (s)	T-B (s)	T-C (s)	T-D (s)	Average partial time (s)
0.01	4.89	4.52	4.83	5.05	4.823
0.02	4.56	3.39	4.26	4.29	4.125
0.03	4.35	3.52	4.61	4.76	4.310
0.04	3.7	3.98	3.61	3.39	3.670
0.05	3.41	3.84	3.52	3.68	3.613
0.06	3.99	3.71	3.83	3.79	3.830
0.07	4	3.39	3.95	4.23	3.893
0.08	3.63	3.72	3.69	3.72	3.690
0.09	3.44	3.35	3.42	3.17	3.345
0.1	3.67	3.79	3.8	3.89	3.788

From the data in Table IV, the average times for each Δh were calculated, and these will be presented as Δ time values in Table V.

In Table V, the inlet velocity (V in) was calculated by dividing Q out by the inlet area (0.00445 m²). These calculations help evaluate the flow behavior by considering height variations and partial times.

TABLE V CALCULATION OF THE INLET VELOCITY FOR TURBULENT FLOW

H accumulated (m)	Δh (m)	Δ time (s)	Δ Volume (m3)	Q outflow (m3/s)	Inflow velocity (m/s)
0.01	0.01	4.823	0.000558	0.000115	0.026
0.02	0.01	4.125	0.000558	0.000135	0.030
0.03	0.01	4.310	0.000558	0.000129	0.029



	1	1		Ī	
0.04	0.01	3.670	0.000558	0.000152	0.034
0.05	0.01	3.613	0.000558	0.000154	0.035
0.06	0.01	3.830	0.000558	0.000145	0.033
0.07	0.01	3.893	0.000558	0.000143	0.032
0.08	0.01	3.690	0.000558	0.000151	0.034
0.09	0.01	3.345	0.000558	0.000166	0.037
0.1	0.01	3.788	0.000558	0.000147	0.033

Table VI was obtained by averaging the outflow rates and inlet velocities from Table V.

TABLE VI

AVERAGES OF OUTFLOW RATE AND INLET VELOCITY FOR TURBULENT FLOW

Q average outflow	m ³ /s	0.00014
V average inflow	m/s	0.03235

For this experiment, it was determined that the density of water at 19°C is 998.75 kg/m³, the average inlet velocity is 0.0324 m/s, and the hydraulic diameter is 0.0347 m. The dynamic viscosity, according to Table A.1 of Robert L. Mott's Fluid Mechanics book, is 0.001 Pa·s. With these values, the calculated Reynolds number was 1073.1007, indicating laminar flow.

W. Autodesk CFD Simulation - Laminar Flow

A laminar flow simulation was performed with the following parameters: material "Water", inlet velocity of 0.01013 m/s, inlet pressure of 30 Pa Gauge, outlet pressure of 0 Pa Gauge, and a mesh size of 0.5. The simulation, with 1000 iterations and laminar turbulence conditions, disabled the temperature and enabled vorticity in the results. For the laminar simulation, the program reached iteration #243.

Figures 8 and 9 show an identical arrangement of the dissipators, demonstrating geometric and kinematic similarity to laminar flow. To confirm dynamic similarity, a detailed analysis of the acting forces would be necessary.

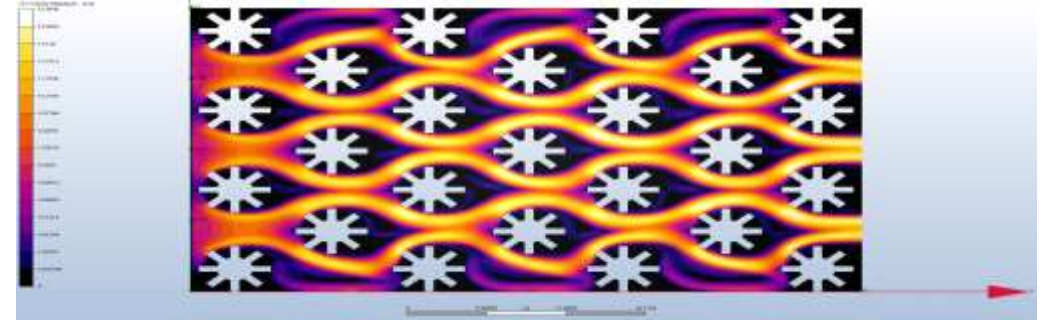


Fig. 8 Laminar flow simulation with a velocity of 0.0101 m/s in Autodesk CFD

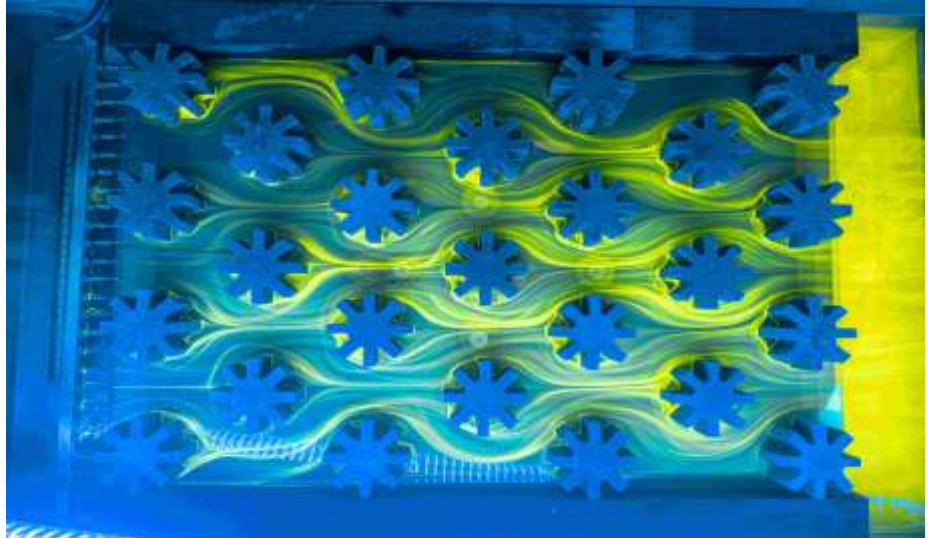


Fig. 9 Laboratory simulations of laminar flow

Figure 10 shows a laminar flow with high pressure at the beginning and low pressure at the end, indicating energy dissipation and flow control.



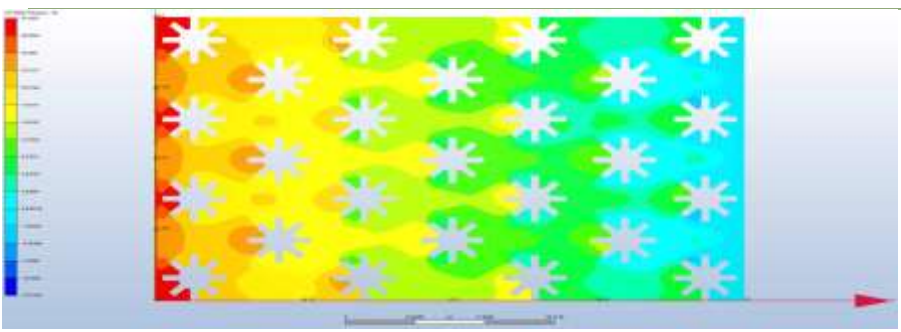


Fig. 10 Static pressure graph in CFD for laminar flow

Figures 11 and 12 reflect a notable geometric and kinematic similarity in the dissipators, associated with a consistent laminar flow. The observed velocity gradients and pressure transitions in the tests validate the dynamic agreement with the CFD model, reinforcing the accuracy of the simulation.

In detail, the images highlight the stagnation point behind the dissipator, the separation point, and the turbulent wake. The pressure increase at the stagnation point generates a significant drag force, aligning with the CFD simulation results, which show elevated pressures in these critical areas. Initially, the fluid adheres to the dissipator surface, but after reaching a critical point, the boundary layer separates, leading to a turbulent wake characterized by considerably lower pressures, a phenomenon also confirmed in the simulation.

The blunt design of the dissipator amplifies the pressure at the stagnation point, increasing the pressure drag. Subsequently, the flow separates rapidly, generating a wide turbulent wake at the rear, a characteristic inherent to blunt bodies. These configurations exhibit higher fluid resistance to maintain adherence to the surface, forming a low-pressure, high-turbulence zone, as observed in the images.

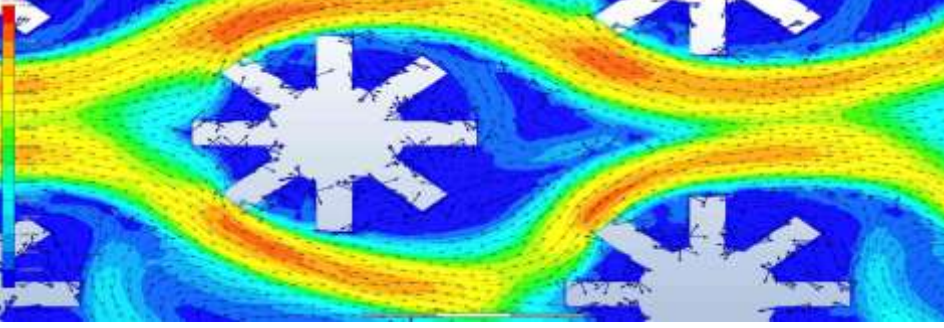


Fig. 11 Water behavior with vectors in Autodesk CFD.

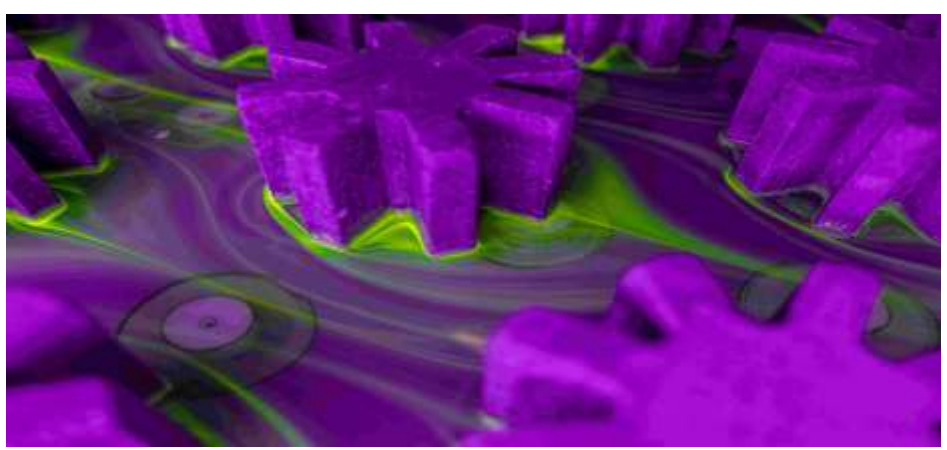


Fig. 12 Detail of laminar flow behavior in the laboratory.

X.Autodesk CFD Simulation – Turbulent Flow

A turbulent flow was simulated with water at 0.032 m/s, 30 Pa inlet pressure, and 0 Pa outlet pressure, using a mesh size of 0.5 and 1000 iterations with the Low Re-k-epsilon model. Temperature was excluded, and vorticity was included in the results. The simulation reached iteration #813 and showed strong kinematic similarity.

Figures 13 and 14 display turbulent flow with vortices, validating the geometric similarity through the uniform arrangement of the dissipators, the kinematics via the streamlines, and the dynamics through the velocity patterns, which match between the CFD simulation and the experimental test. The high flow velocity makes precise capture in the images challenging; however, the use of a fluorescent fluid aids in visualization. The high pressures impacting the dissipators generate turbulent wakes and low-pressure zones downstream, highlighting the vorticity of the flow and making these wakes more visible.





Fig. 13 Simulation with a velocity of 0.03235 m/s in Autodesk CFD.

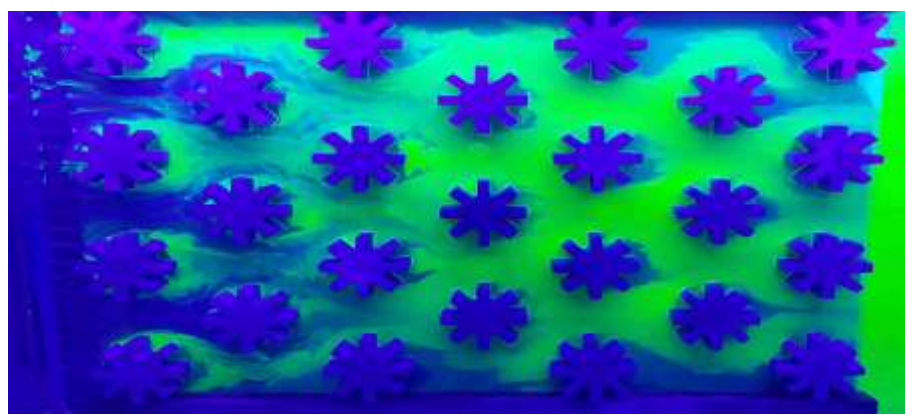


Fig. 14 Laboratory simulations of turbulent flow

Figure 15 illustrates the pressure distribution along the flow, highlighting areas of high pressure at the beginning, caused by the impact at a high initial velocity, followed by a gradual decrease towards the end due to the energy dissipation process.

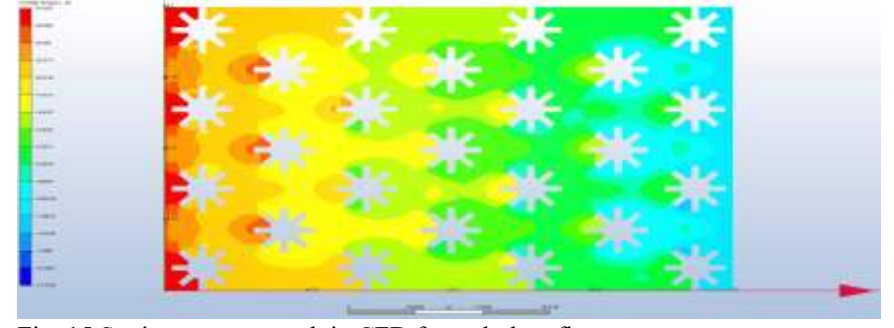


Fig. 15 Static pressure graph in CFD for turbulent flow

CONCLUSIONS

The comparative analysis between the experimental laboratory test and the CFD simulation showed a strong kinematic similarity, reflected in the flow lines, suggesting that factors such as temperature, water density, and viscosity have minimal impact on the results. However, small discrepancies were observed in the simulations due to unmodeled factors, such as bubbles, particles in the water, and environmental vibrations. Temperature also influenced viscosity, causing slight variations between the experimental and simulated results under ideal conditions. Both approaches showed consistency in flow patterns and pressure behavior, confirming the predictive capability of the CFD simulation in laminar flow.

The research highlights the importance of controlling forces such as drag and lift in the performance of the energy dissipation device, with reduced drag improving energy efficiency and controlling lift ensuring design stability. Geometric adjustments optimized the dissipator, emphasizing the relevance of precision in geometry and variable control during laboratory tests. This combined experimental and simulated approach provides a robust methodology for improving energy dissipation designs, with significant implications for flood control, such as mudslides (huaycos) in Peru, advancing hydraulic engineering and water flow energy management.

REFERENCES

[1] P. I. Silva Rubio y C. A. Nieto del Valle, «Sequía por cambio climático como factor de vulneración del derecho humano al agua potable y saneamiento: una visión desde México», Brazilian Journal of Development,



- vol. 10, no. 10, pp. 01-14, 27 de septiembre de 2024. [En línea]. Available: https://ojs.brazilianjournals.com.br/ojs/index.php/BRJD/article/view/73705/51562
- [2] C. Tipan-Torres, «Impacto del Cambio Climático en los Ecosistemas Forestales: Un Análisis Exploratorio», Horizon Nexus Journal, vol. 2, no. 3, pp. 1-17, 2024. [En línea]. Disponible en: https://horizonnexusjournal.editorialdoso.com/index.php/home/article/view/4/9.
- [3] K. B. Lino Inocencio, «Estimación de parámetros para el cálculo de riesgo de inundación a partir de modelos climáticos en la confluencia de los ríos Huertas y Huallaga, ciudad de Ambo Huánuco», Tesis para optar el título profesional de Ingeniera Civil, Universidad de Huánuco, Huánuco, Perú, 202. [En línea]. Disponible en: https://repositorio.udh.edu.pe/bitstream/handle/20.500.14257/5094/Lino%20Inocencio%2c%20Keily%20Briset.p df?sequence=1&isAllowed=y.
- [4] P. Depaula, «Huaycos en el distrito limeño de Lurigancho-Chosica: urbanización, vulnerabilidad social, cultura y resiliencia comunitaria», Revista ConCiencia EPG, vol. 4, no. 1, pp. 78-91, 2019. [En línea]. Disponible en: https://doi.org/10.32654/CONCIENCIAEPG.4-1.5
- [5] S. V. del P. Huarcaya Soto y C. A. Pineda Miranda, «Evaluación de impacto ambiental de alternativas de mitigación frente a inundaciones y huaycos en épocas de avenidas en la subcuenca Santa Eulalia, cuenca del río Rímac», tesis de pregrado, Facultad de Ciencias e Ingeniería, Pontificia Universidad Católica del Perú, Lima, Perú, 2024. [En línea]. Disponible en:
- https://tesis.pucp.edu.pe/repositorio/bitstream/handle/20.500.12404/28713/HUARCAYA%20SOTO_PINEDA%20MIRANDA.pdf?sequence=1&isAllowed=y
- [6] E. P. Camarena Salazar, «Hurto de los aros de acero de la malla geodinámica en el distrito de Lurigancho—Chosica a causa de la falta de información sobre las medidas de seguridad y prevención ante un huayco», trabajo de investigación para optar el grado de Bachiller en Arte y Diseño Empresarial, Facultad de Humanidades, Universidad San Ignacio de Loyola, Lima, Perú, 2020. [En línea]. Disponible en: https://repositorio.usil.edu.pe/server/api/core/bitstreams/d28b5bf2-1335-4bf2-a9f4-e9cde01f1b94/content
- [7] K. Z. Gutierrez, «Medidas de seguridad antes, durante y después de un huaico», MAPFRE Perú, 8 de noviembre de 2023. [En línea]. Disponible en: https://www.mapfre.com.pe/viviendo-en-confianza/hogar/medidas-de-seguridad-antes-durante-y-despues-de-un-huaico/
- [8] Software Autodesk Inventor | Obtener precios y comprar el producto oficial Inventor 2025. (s. f.). [En línea]. Disponible en: https://www.autodesk.com/es/products/inventor/overview?term=1-YEAR&tab=subscription
- [9] «Autodesk CFD Software | Get prices & Buy Official CFD», Autodesk. [En línea]. Disponible en: https://www.autodesk.com/products/cfd/overview?term=1-YEAR&tab=subscription.
- [10] J. M. de Vehi Sarrazin, "Mallado de geometrías complejas mediante CFD," Trabajo de Final de Grado, Grado en Ingeniería en Tecnologías Industriales, Universitat Politècnica de Catalunya, Barcelona, España, abril 2016. [En línea]. Disponible en: https://core.ac.uk/download/pdf/81577803.pdf
- [11] R. L. Mott y J. A. Untener, Mecánica de fluidos, 7a ed. Pearson, 2015. [En línea]. Disponible en: https://www.academia.edu/37998666/PDF Mecanica de Fluidos 7a ed Mott
- [12] E. D. dos Santos, C. M. Xavier, y A. P. Petry, "Estudio numérico de flujos turbulentos isotérmicos en canales y flujos laminares con convección mixta en cavidades," Información Tecnológica, vol. 22, no. 1, pp. 71-78, 2011. [En línea]. Disponible en: https://www.revistainformaciontecnologica.com
- [13] O. G. Valentín-Paza y M. A. Canales-Alvarado, "Comparación entre el efecto hidrodinámico debido al empuje del agua, sobre pilas de puentes, considerando flujo laminar y flujo turbulento," en VII Jornadas de Ingeniería del Agua (JIA 2023), Cartagena, España, 18-19 de octubre de 2023. [En línea]. Disponible en: https://repositorio.upct.es/server/api/core/bitstreams/e42172e1-be52-4653-ae8b-db7b28a0642d/content
- [14] S. O. Ortiz Vera, «Similitud hidráulica de sistemas hidrológicos altoandinos y transferencia de información hidrometeorológica», tesis doctoral, Doctorado en Recursos Hídricos, Escuela de Posgrado, Universidad Nacional Agraria La Molina, Lima, Perú, 2016. [En línea]. Disponible en:
- https://repositorio.lamolina.edu.pe/server/api/core/bitstreams/821afda7-e82a-48bc-b260-ba4c20577b5e/content [15] G. Aldana y J. Pérez, «Simulación del patrón de flujo y del tiempo de retención hidráulico en lagunas de estabilización y reactores anaerobios de flujo ascendente (RAFA) a través de un modelo físico», SciELO Venezuela. [En línea]. Disponible en: https://ve.scielo.org/scielo.php?pid=S0254-07702010000100007&script=sci_arttext
- [16] J. Cid Solé, «Estudio experimental de la influencia del estrato rocoso en la forma del foso de erosión producida por jet en salto de esquí», Departament d'Enginyeria Hidràulica Marítima i Ambiental, Universitat Politècnica de Catalunya, 1 de diciembre de 2004. [En línea]. Disponible en: http://hdl.handle.net/2099.1/3296
- [17] Y. A. Çengel y J. M. Cimbala, Mecánica de fluidos: Fundamentos y aplicaciones, 2a ed. McGraw-Hill, 2010. [En línea]. Disponible en:
- https://www.academia.edu/25669790/Mecanica_de_Fluidos_Fundamentos_y_Aplicaciones_Yunus_Cengel_y_Jo hn Cimbala Primera Edicion
- [18] M. E. Pérez Segura, A. T. Brewer, y S. Preidikman, "Programación orientada a objetos aplicada a simulaciones de flujos dominados por vorticidad Parte 1: Aspectos de implementación," Mecánica Computacional, vol. XXXVII, pp. 1747-1756, Asociación Argentina de Mecánica Computacional, Santa Fe, Argentina, 5-7 de noviembre de 2019. [En línea]. Disponible en: https://cimec.org.ar/ojs/index.php/mc/article/view/5993/6038